Interconnected Multilayer Model to Highlight Condensation and Expansion Mechanisms in a Retinal Connectome

Robin Duvoisin

This manuscript was compiled on February 21, 2024

A connectome serves as a complete map detailing the neural connections within a brain network. To elucidate the intricate relationship between function and structure, these maps are depicted as graphs, with nodes representing cell bodies and edges symbolizing the communication between cells. However, the conventional representation oversimplifies the actual network structure by treating all neurons as uniform entities. In this study, we address this limitation by introducing a multilayer model. This model involves partitioning the network into smaller subgraphs based on cell type classifications and incorporating these subgraphs into distinct layers. While traditional topological algorithms for multilayer networks are tailored for multiplex models, where nodes remain identical across layers, our investigation focuses on interconnected models, where layers contain a unique set of nodes. The main idea of this paper is to present a topological analysis pipeline tailored for interconnected models. We applied this method on a mouse retina connectome to extract cell type-specific topological properties. Our findings reveal that the multilayer framework unveils previously hidden features, including condensation, and unexpected expansion of the information flow. These findings contribute to a deeper comprehension of retinal computation, emphasizing the imperative need for further exploration of methodologies for topological analysis in interconnected multilayer models.

Interconnected Multilayer Network | Retinal Computation | Connectome

Significance Statement

The prevailing framework to represent networks with multiple distinct layers of interactions, is the multilayer model. The analysis of the model is mainly developed for the multiplex subtype, where nodes remain identical across layers. To our knowledge, this study pioneers extending these algorithms to an interconnected multilayer model, relaxing the constraint of the multiplex subtype. Applied to a mouse retina brain network, our approach uncovers unique properties, including a cell-type-specific hub and highlighting particular information flow dynamics in retinal processing. This innovative pipeline enhances our understanding of interconnected multilayer networks.

The human brain, with approximately 10^{11} neurons and a connection matrix of size 10^{100}(1), poses a modeling challenge. Hence, scientists initially studied smaller networks, including mice's sensory systems. The visual system is ideal, consisting of well-known, spatially separated cell types organized into layers. Additionally, retinal computation is within a preferential range of complexity, with the ability to extract special features of a visual scene, including color or luminance contrast, without extensive connections to other neural systems (2). To better understand this computation, scientists generate connectomes, which are comprehensive representations of neuron structures and their connections, called synapses (3). These massive datasets are obtained using imaging methods like electron microscopy and staining techniques to reconstruct the wiring diagram (4). In this article, we further investigate the dataset with 950 neurons of mice's visual system, constructed by Helmstaedter et al. (3). The connectome is converted into a network, where nodes represent cell bodies and edges represent communication channels between cells.

Analyzing brain networks is necessary to observe if visible macroscopic behavior, such as retinal computation, is attributed to inherent topological properties of microscopic units, such as a group of cells (1). In this paper, we aim to understand the relationship between the type of the cell and its impact on the dynamics of the network. For this purpose, selecting an appropriate model is crucial to observe localized behavior without generating oversimplification. We opted for a multilayer model with layers representing the types of cells. This model enables us to observe structural differences between cell types while preserving the actual layering structure of the visual system. Previous studies utilizing the multilayer model with connectomes have already shown significant results (4)(5). Using the layers as a representation of different communication channels, such as neurotransmitters and neuromodulators, revealed that two distinct layers give the network the ability to adapt to the environment (5) and to maintain a form of memory (4). Additionally, both studies confirmed the presence of central high-degree hubs, called rich-club, which play a prominent role in regulating the network while providing an efficient

IA tools such as Chatgpt or Grammarly have only been used for text correctness or clarity improvement.

E-mail: robinarnaud.duvoisin@uzh.com

information transfer due to their short path lengths with the rest of the network (4)(5). Our model differs from previous studies, which predominantly utilized the multiplex subtype, where nodes remain identical across layers. In our model, termed an interconnected multilayer representation (6) or interacting network (7), a node can only be represented in one layer. We suspect an overrepresentation of the multiplex model in connectome transformations due to the lack of equations describing interconnected multilayer topological analysis. Effectively, most papers providing insight into multilayer analysis focus on frameworks for multiplex models without generalization for the interconnected multilayer (6)(8)(9).

In this paper, the first objective is to demonstrate that the interconnected multilayer representation of the connectome is more optimal than a monolayer model. The second goal is to generalize the topological analysis pipeline from multiplex to interconnected multilayer networks. This will be achieved through the computation of different properties such as the rich-club and local clustering coefficient. Our results show that, through appropriate modeling, we have been able to reveal localized dynamics, such as feedforward/feedback patterns and information expansion/condensation, that are hidden in an oversimplified monolayer model. We highlighted the presence of a layer-specific rich-club hub. All of these assertions are made in comparison to a null model, characterized by randomized graphs that maintain a similar degree distribution within and between the layers as observed in the original network. To facilitate comprehension of forthcoming results, we will begin by providing a brief overview of the retinal network and its functionality.

1. Mulitlayer Representation

A. Description of the Retinal Network. In a broader context, sensory organs play a crucial role in capturing and transducing physical properties from the surrounding environment. The signal is then transmitted to the sensory cortex, where neural computation extracts a meaningful representation of the world to enable behavioral adaptation of the organism. In the visual pathway, the mouse retina consists of around 6.4 million light-sensitive receptor cells and around 2000 ganglion cells responsible for transferring information to the central nervous system (CNS) (10). As mentioned in the article from Nassi J. et al. (2), this extreme difference in cell density suggests the necessity to condense the signal for a bottleneck passage in order to reach higher neural systems. Given the fixed surface of reactivity determined by eye size, a trade-off emerges between having more optical nerves for increased information transmission to the CNS and capturing fewer photons due to limited space for photoreceptor cells (2). The retina network is required to condense and decompose inputs to generate parallel specialized pathways for optic nerves, containing information such as luminance and color contrasts (2). We will now outline the complete retinal processing pathway in a step-by-step manner.

Initially, photons hit a photoreceptor cell, and the signal is transduced through a change in the cell membrane potential. Bipolar cells (BC), forming the second layer, detect this modification. Bipolar cells then connect with ganglion cells (GC) directly or indirectly through amacrine cells (AC) (see schematic in the Appendix 9). Ganglions generate optic nerves that reach the cortex. In this article, we will focus on the Inner Plexiform Layer (IPL) containing connections between amacrine, bipolar, and ganglion synapses (11). It is important to note that, unlike typical neurons, a change in the membrane potential of a retinal cell does not necessarily induce an action potential (i.e. a non-linear response releasing chemical informative substances, named neurotransmitters, if a threshold is reached). Instead, multiple retinal cells communicate through gap junctions (12)(13), enabling rapid electrical transmission between cells without depending on a threshold (11). As the central nervous system relies mostly on action potentials, there is a transfer of information space from gap junctions to classical synaptic neurotransmitter release.

To comprehend the complete computation made by the retinal network, we can compare the difference between the input at the first stage and the output at the last stage of the process. Photoreceptor cells respond to a set of localized photons on a surface similar to their cell diameter. In contrast, Ganglion cells generate an output if they are excited by a larger light pattern with a Difference of Gaussian structure. Ganglion cells can intricately integrate two circular receptive fields: one responding to an increase and one to a decrease in light intensity, defining a contrast (2). This processing is accomplished by comparing the input from one photoreceptor with its surroundings and averaging/weighting the information based on the input's location. For a visual representation of this concept, please refer to the image illustrating the receptive field of a ganglion cell in Appendix 10. With a deeper understanding of the processing abilities and structure of the retinal network, we will now present our argument regarding the choice of the multilayer model.

B. "Why not a modular network?". After deciding to represent the retinal network with nodes corresponding to cell bodies and synapses as edges, our intial intuition, based on the retina's description, led us to consider a monolayer modular network, with a module dedicated to each cell type. In network science, a modular model is defined as a network containing groups of nodes with distinct properties that are more connected together compared to the rest of the network (14). However, a brief modular analysis of the network, illustrated in the image 11 & 12, reveals that separation based on edges connections did not align with distinct cell types. We assert that a multilayer representation would be a more appropriate model because each layer is characterized by different dynamics and properties. First, we observe that all cell types within the network influence the retinal processing at different stages. Furthermore, these cell types utilize various communication methods, involving distinct neurotransmitters (e.g. Glutamate for BC and GC and GABA for Amacrine (6)) and different types of channels (only gap junctions for BC, action potential for GC and both for Amacrine cells (15)). Additionally, it has been demonstrated that the extracellular space varies significantly (i.e. five times greater in a few micrometers) between the layers. The amount of extracellular space available can modify the osmotic properties of the environment, leading to different diffusion constants for neurotransmitters, equivalent to having different time dynamics (16). Finally, the cell types operate on different processing planes, with Amacrine cells being more

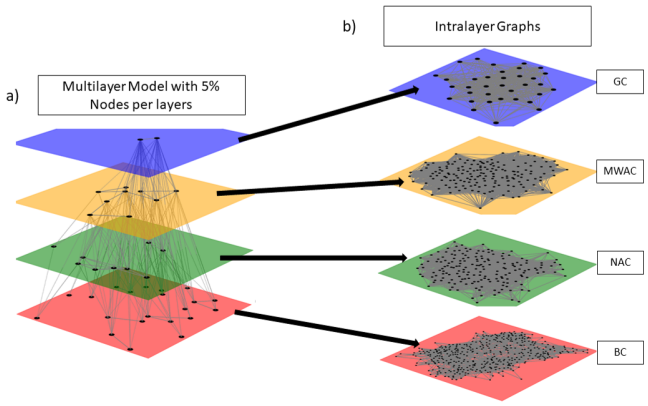

Fig. 1. a) Partial representation of the interconnected multilayer model with 5% of nodes per layer randomly selected. The partial depiction provides insight into variations in edge density within the layers. A complete table providing the numbers of edges and nodes per layer is provided in the Appendix 1. b) Complete intralayer graphs with GC = ganglion cells, MWAC = medium/wide-field amacrine cell, NAC = narrow amacrine cell, BC = bipolar cell.

horizontally oriented, establishing broad connections from different locations of the visual field compared to Bipolar and Ganglion cells, which are more vertically connected and specialized to one location of the visual field (Appendix Image 9). For all the aforementioned reasons, we opted for an undirected multilayer representation with 4 different types of layers (Image 1), one for each cell type with a separation of the amacrine cell into two groups distinct by their spreadability, the narrow-field (NAC) and the medium/wide-field (MWAC) as it has been done in the initial article on the connectome (4). To analyze this network, it is necessary to characterize topological equations and definitions within the monolayer model before extending it to a multilayer representation. In the following section, we will introduce the rich-club and the local clustering coefficient, which will be employed to describe the network properties in later sections.

C. Mathematical description. A network graph G is characterized by a set of nodes $V = \{v_i | i \in [1, \dots, N]\}$ and a set of edges $E = \{e_{ij} | (i,j) \in V \times V\}$ (9), represented by the weighted adjacency matrix $A \in \mathbb{R}^{\mathbb{N}\times\mathbb{N}}$:

$$A_{ij} = \begin{cases} w_{ij}, & \text{Weight of the edge between node } i \text{ and } j \\ 0, & \text{else} \end{cases}$$

Building upon the work by Boccaletti et al. (6), we extent the definition to the multilayer model with $\mathfrak{M} = (\mathfrak{G}, \mathfrak{E})$ for $\mathfrak{G}$ a set of graphs in M layers $\mathfrak{G} = \{G_\alpha = (V_\alpha, E_\alpha) | \alpha \in [1, \dots, M]\}$ and $\mathfrak{E} = \{E_{\alpha\beta} \subseteq V_\alpha \times V_\beta | (\alpha, \beta) \in [1, \dots, M], \alpha \neq \beta\}$ a set of edges interconnecting the different layers α and β. The Latin letters (i, j) represent the monoplane indices, and the Greek letters (α, β) are associated with the layer indices (6). $\mathfrak{E}$ represents the interlayer connections, and E_α represents the intralayer connections (6). The supra-adjacency matrix A contains the intralayer symmetrical matrix $A^{[\alpha]} \in \mathbb{R}^{\mathbb{N}_\alpha \times \mathbb{N}_\alpha}$ for $(i, j) \in [1, \dots, N_\alpha]$ and $\alpha \in [1, \dots, M]$:

$$a_{ij}^{\alpha} = \begin{cases} w_{ij}^{\alpha}, & \text{Weight of } (v_i^\alpha, v_j^\alpha) \in E_\alpha \\ 0, & \text{else} \end{cases}$$

And the interlayer matrix $A^{[\alpha\beta]} \in \mathbb{R}^{\mathbb{N}_\alpha \times \mathbb{N}_\beta}$ with $(\alpha, \beta) \in [1, \dots, M], \alpha \neq \beta$ for $i \in [1, \dots, N_\alpha], j \in [1, \dots, N_\beta]$:

$$a_{ij}^{[\alpha,\beta]} = \begin{cases} w_{ij}^{[\alpha,\beta]}, & \text{Weight of } (v_i^\alpha, v_j^\beta) \in E_{\alpha,\beta} \\ 0, & \text{else} \end{cases}$$

During the analysis, we will compare a global monolayer representation written $\mathcal{G} = (\mathcal{V}, \mathcal{E})$ with the multilayer one. The union of inter- and intralayer connections forms the set of monolayer edges, and the union of nodes across all layers will generate our set of monolayer nodes. According to Boccaletti et al. (6), the relation between the two is noted as:

$$\mathcal{E} = \left(\bigcup_{\alpha=1}^{M} E_\alpha \right) \bigcup \left(\bigcup_{\substack{\alpha,\beta=1 \\ \alpha\neq\beta}}^{M} E_{\alpha\beta} \right) \qquad \mathcal{V} = \bigcup_{\alpha=1}^{M} V_\alpha$$

Multilayer models encompass various subtypes, with one simplified version being the multiplex model, where nodes are identical across all layers, leading to $\mathcal{V} = V_\alpha$ and $N = N_\alpha \forall \alpha \in [1, \dots, M]$. This leads to inter- and intralayer adjacency matrices with the same dimensions, denoted as $A_{mulitplex} \in \mathbb{R}^{\mathbb{NM}\times\mathbb{NM}}$, facilitating linear algebra formulas (9). An illustration depicting the difference between the two models can be found in Appendix 13. Now, we aim to extend the multiplex definitions of topological properties, including overlap degree, rich-club, and local clustering coefficient, found in scientific articles (6)(8) to an interconnected model.

The degree of a node i is defined as the number of edges in contact with v_i. In a multilayer network, the presence of layers degrees allows us to define the overlapping degree as the sum of interlayer and intralayer degrees (9). This is calculated using Equation 1 on the supra-adjacency matrix A, with N_{tot} as the total number of nodes in the network, M as the number of layers, and N_α as the number of nodes in the layer α.

$$N_{tot} = \sum_{\alpha=1}^{M} N_\alpha \qquad Overlap_i = \sum_{j=1}^{N_{tot}} A_{i,j} \qquad [1]$$

If high-degree nodes tend to be more connected together than the null hypothesis, we refer to them as rich-club. For each degree k, the coefficient $\Omega(k)$ is computed through the division of the number of edges E_k, connecting two nodes having degrees greater than k, with the number of nodes N_k, having degrees greater than k (Equation 2). The coefficient is normalized by an average of the results obtained by a random network that conserves the degree distribution (9). To extend the calculation to the multilayer model, we compute the coefficient using the adjacency matrix $A^{[\alpha,\beta]}$ and vectors indicating whether the node degrees between layers α and β are greater than k. These vectors are denoted as $bool\_deg^\alpha \in \mathbb{R}^{N_\alpha \times 1}$ and $bool\_deg^\beta \in \mathbb{R}^{1 \times N_\beta}$, where N_α represents the number of nodes in the layer α (similar for layer β). $E_k^{[\alpha,\beta]}$ represents the number of edges between the two layers connecting nodes with degrees greater than k, and the numbers of nodes with degrees greater than k are denoted as N_k^α and N_k^β respectively. A case-specific modification is required for the matrix-centered Equation 5, where the counting of edges and nodes occurs twice for the intralayer case (i.e. symmetrical matrices).

$$\Omega_{Monolayer}(k) = \frac{2E_k}{N_k(N_k-1)} \quad [2]$$

$$bool\_deg^{\alpha} = \begin{cases} 1, & \text{if } \sum_{j=1}^{N_\beta} A_{i,j}^{[\alpha,\beta]} > k \\ 0, & \text{else} \end{cases}$$

$$N_k^{\alpha} = \sum_{i=1}^{N_\alpha} bool\_deg_i^{\alpha} \quad [3]$$

$$E_k^{[\alpha,\beta]} = (bool\_deg^{\alpha})^T \times A^{[\alpha,\beta]} \times (bool\_deg^{\beta})^T \quad [4]$$

$$\Omega(k) = \begin{cases} \frac{2E_k^{[\alpha,\beta]}}{(N_k^{\alpha}+N_k^{\beta})((N_k^{\alpha}+N_k^{\beta})-1)}, & \text{for } \alpha \neq \beta \\ \frac{E_k^{[\alpha,\beta]}}{(N_k^{\alpha})((N_k^{\alpha})-1)}, & \text{for } \alpha = \beta \end{cases} \quad [5]$$

In the monolayer model, the local clustering coefficient, C_i, serves as an indicator to determine whether "the friend of my friend is also my friend", as defined in Newman's book (17). Put simply, the local clustering coefficient of the node v_i is defined as the ratio of connected pairs of neighbors of v_i to the total number of possible pairs of neighbors, equivalent to $\frac{1}{2}k_i(k_i-1)$, where k_i represents the degree of node i (9). Defining a similar parameter for the multilayer model is challenging because the meaning of a friendship triangle between layers varies depending on the model (8). In the multiplex model, where a node v_i appears in multiple layers, the parameter is measured through the generation of a projection network that condenses the connections of multiple layers (for more information, refer to the review by Boccaletti et al. (6)). In our model, we have chosen to distinguish three types of local clustering parameters. The first one corresponds to a horizontal coefficient, measuring the trivial monolayer equation on the intralayer graph. The second and third one emerges from the dataset's particular feature: the information flow. As layers also represent stages of processing, a triangle containing one node in a high-level layer and two nodes in a deeper one is considered as an "expansion" of the information. In contrast, a triangle with two nodes in a high-level layer converging to one node in a lower layer is defined as condensation (Image 2). For the multilayer model, the total number of possible pairs of neighbors is layer-specific, equivalent to $\frac{1}{2}k_i^{[\alpha\to\beta]}(k_i^{[\alpha\to\beta]}-1)$, where $k_i^{[\alpha\to\beta]}$ represents the degree of node i in layer α connecting to layer β. Equation 8 defines the expansion clustering coefficient from the high-level layer α containing node i to layer β. The condensation clustering coefficient of the same system would have an equivalent formula with $[\beta \to \alpha]$.

$$C\_monolayer_i = \frac{Nbr\_connected\_pairs\_of\_neighbors\_of\_i}{\frac{1}{2}k_i(k_i-1)} \quad [6]$$

$$k_i^{[\alpha\to\beta]} = \sum_{j=1}^{N_\beta} A_{i,j}^{[\alpha,\beta]} \quad [7]$$

$$Exp\_C_i^{\alpha\to\beta} = \frac{2Nbr\_Expansion\_Triangles}{k_i^{[\alpha\to\beta]}(k_i^{[\alpha\to\beta]}-1)} \quad [8]$$

To evaluate the significance of the above-mentioned network features, a comparison with a null graph model is essential. In the study conducted by Bentley et al. (5), the double-edge swap algorithm was employed to generate randomized versions of a multiplex connectome. The primary objective of this algorithm is to exchange two existing edges, thereby altering the network's structure while preserving the degree distribution. Specifically, the two selected edges $[(a \to b),(c \to d)]$ are transformed into $[(a \to d),(c \to b)]$. The extension of this algorithm to an interconnected multilayer matrix is possible by selecting nodes from different layers. Let's define layers α and β with the respective interadjacency matrix $A^{[\alpha\beta]}$. For nodes $(x,y) \in [1,\dots,N_\alpha]$, $(u,v) \in [1,\dots,N_\beta]$ and the original set of edges $(E_{\alpha\beta})_0 = [(x,u),(y,v)]$. The double-edge swap algorithm transforms the set into $(E_{\alpha\beta})_1 = [(x,v),(y,u)]$ only if these connections were not present in the original version $(E_{\alpha\beta})_0$ to prevent the generation of a multigraph (i.e. multiple connections between two nodes). We will now present the results obtained when applying these topological analyses to the retinal connectome network.

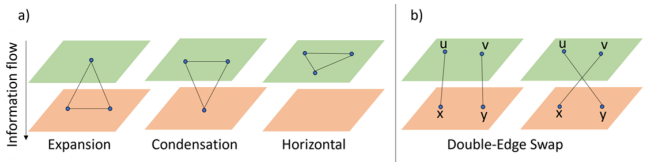

Fig. 2. a) The three types of "friendship" triangles that define the local clustering coefficient. The arrow represents the information flow, with the green layer at an early stage of the retinal processing relative to the brown layer. From left to right, we observe the expansion and the condensation effect in an interlayer graph. The last image represents the trivial horizontal monolayer category. b) The double-edge swap on a multilayer graph. The left side shows the initial graph, and the right side shows the same graph after the transformation.

2. Results

To guide our topological analysis, we initially explored the non-weighted overlap distribution between layers to provide a brief network structure overview. The image 3 compares the degree distribution curve in a monolayer model to the overlap degree distribution in the multilayer model. The monolayer representation, conclusively, fails to capture distinct dynamics between cell types, unlike the multilayer model. In the Appendix, we compared the weight distribution between layers, further affirming the inability of a monolayer model to discern layer-specific dynamics. Image 3 and Appendix image 15 reveal varying dynamics between the two amacrine cells, reinforcing our initial hypothesis to segregate the group.

After confirming the advantages of the multilayer framework, we explored interlayer topological properties, focusing on the degree distribution between layers (Appendix image 17). The graph unveils two types of information flow. The degree distributions of connections from the last step of retinal processing (i.e. Ganglion) to the first step (i.e. Bipolar) show a short variation near the peak, representing backward information flowing. In contrast, degree distributions of the second information flow (i.e. from Bipolar to Ganglion) have a larger variation. We named these mechanisms feedback and feedforward, illustrated in the image 4. As previously introduced, there are three main pathways for the forward information flow, BC→MWAC→GC, BC→NAC→GC and

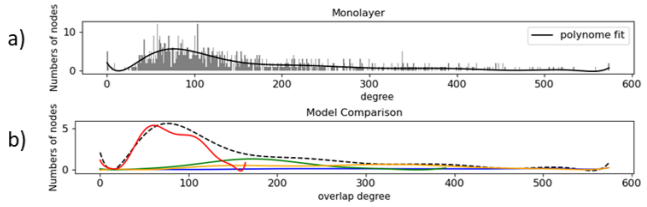

Fig. 3. a) The histogram depicts the degree distribution of the monolayer model, with the dark line representing a polynomial fit of the distribution. b) The linear fitting functions extracted from the overlap degree distribution for each layer in solid line (red = BC, green = NAC, yellow = MWAC, blue = GC). The linear fitting function from the graph a) in the dashed black line. The graph illustrates that a monolayer representation fails to capture all the dynamics of the network. bc=bipolar cell, nac= narrow-field amacrine, mwac=medium/wide-field amacrine,gc= ganglion cell.

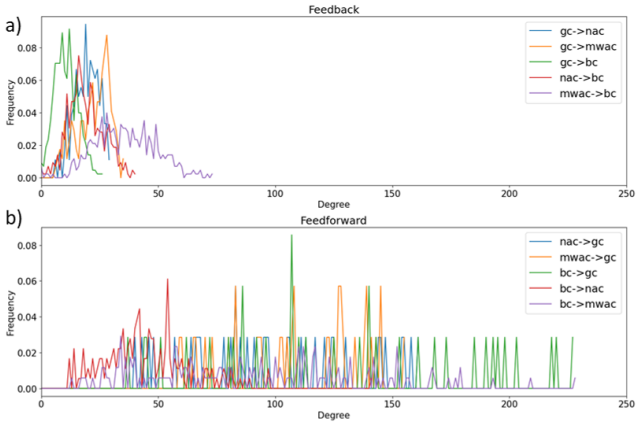

Fig. 4. Collection of intralayer degree distributions. a) Representation of the feedback patterns. The curves originate from the upper triangular part of the complete 4x4 layers across layers degree distribution image, visible in the Appendix 17. All of these degree distributions exhibit a short variation near the peak, representing the information flow from ganglion cells to bipolar cells. b) Representation of feedforward patterns. The curves originate from the lower triangular part of the complete Appendix Image 17. The information flows from the bipolar cells to the ganglion cells, and these distributions are characterized by being long-tailed.

BC→GC. Each pathway controls information differently due to its unique collection of degree distribution.

To confirm these three types of information flow pathways, we analyzed three types of local clustering coefficients (Image 2). Summarizing the properties visible in the Appendix image 20, MWAC and GC coefficients are consistently relatively close to the null hypothesis. In contrast, NAC and BC tend to have higher coefficients than the randomized network. Finally, the condensation clustering is higher for the MWAC than NAC.

Analyzing the rich-club coefficient requires computing a set of randomized matrices for normalization. The Mat-D-E-S-Algorithm implementation for randomizing asymmetric matrices is depicted in the Appendix image 18. The results exhibit similarities to a double-edge swap transformation using the Networkx package in Python (18), affirming the correctness of our algorithm. Rich-club nodes in our network are present in intralayer matrices. The most notable set is in the BC layer for nodes with degrees greater than 32, while a smaller set is visible for the NAC with degrees in the range of $[58, 64]$ (Image 5). These hubs must play a crucial role in regulating information flow and comparing inputs from different locations, given their high connectivity.

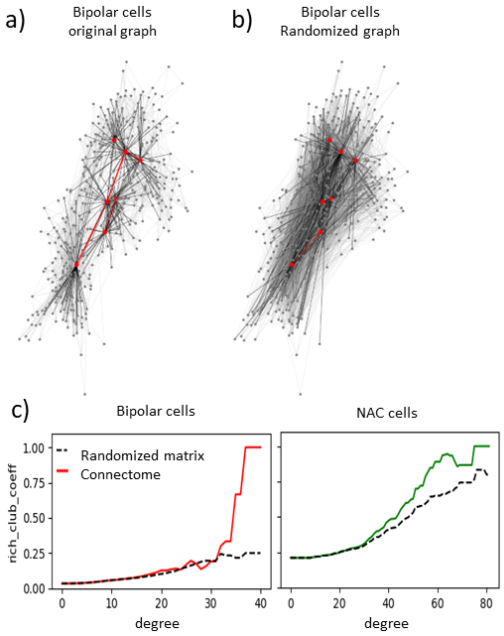

Fig. 5. a) The graph depicts the bipolar cell intralayer network with the rich-club outstanding node in red (degree exceeding 32). The edges between one of the red nodes and its neighbors are in black, while the edges connecting two high-degree nodes are in red. b) A similar graph after the network underwent a double-edge swap transformation. The connections between rich-club nodes are drastically reduced. c) The original rich-club coefficient of the connectome and the average of the same coefficient derived from partially randomly generated graphs. The left plot represents the bipolar cell, and the right one represents the narrow amacrine cells.

3. Discussion

Through the study, we unveiled layer-specific network features, including a feedforward mechanism characterized by a heavy-tailed degree distribution, and a feedback mechanism characterized by a sharper degree distribution. It is reasonable to consider that the variation in the size of the layer may be responsible for these distinct shapes. For instance, there is a 1/10 ratio between the number of Ganglion and Bipolar cells, resulting in a smaller set capable of producing feedback. However, it is important to highlight that the distribution pattern stays consistent even when considering sets with smaller size variations, such as the connection between Amacrine and Bipolar cells, contradicting the first intuition. Furthermore, the feedforward mechanism varies between layers, and we hypothesize that these distribution functions inform about condensation and expansion factors in the network. Another valid question is: "Why can we relate the number of connections with the retinal processing?". The answer lies in the retinal processing Appendix schematics 10. The final product of the computation is a weighted sum of the inputs that can be approximated by a Difference of Gaussian. Modifying the number of edges changes the sum, leading to different Gaussian forms (tighter, more spread,...). Indeed, we hypothesize that the representation of the Ganglion receptive field in Appendix image 10 is incorrect. Instead of a slow linear compression of inputs until it matches the bottleneck size generated by the ganglion, alternative cell-type-specific mechanisms, such as expansion, come into play. After compiling the results obtained from the degree

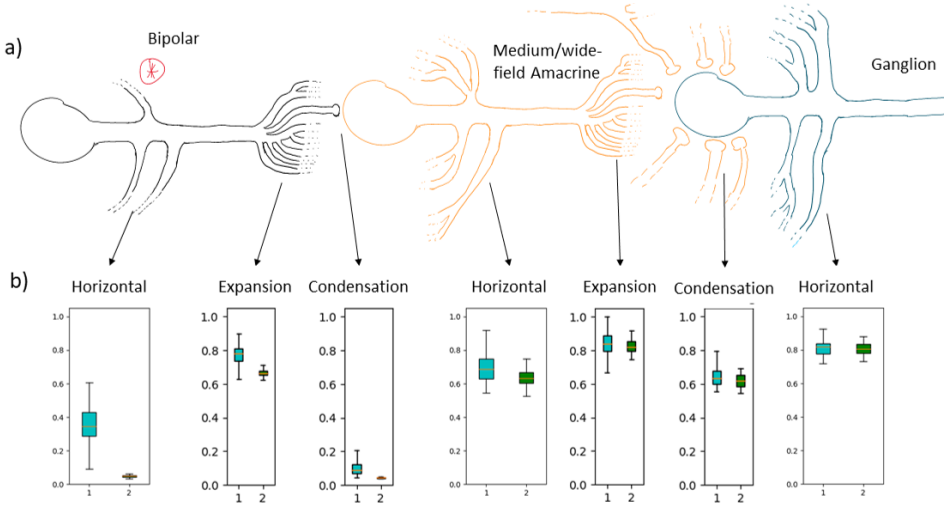

Fig. 6. The image illustrates a potential information flow pathway from the Bipolar to the medium/wide-field Amacrine terminating in the Ganglion. a) Schematic of the specificity of the pathway. b) The variation of the local clustering coefficient during the pathway. In the boxplot, the first column represents the original network, and the second is the average of randomized graphs. The MWAC pathway uniquely exhibits a late high condensation coefficient, emerging only during the connection with GC. All specificities deviating from the null model are marked with a red star in (a), though they do not represent statistical evidence. The clustering coefficients in (b) are converted into the number of connections shown in (a), providing a conceptual idea of connections.

distribution and the local cluster coefficient, we are able to describe two main information flow pathways. The MWAC pathway (Image 6) condenses information during the transfer to Ganglion cells. This implies a high number of node pairs in MWAC merging into one specific Ganglion, a mechanism correctly represented in the schematic in Appendix 10. This condensation step depends on this cell specific subtype, and narrow Amacrine cells do not exhibit this behavior. Image 7 shows the topological properties of the NAC pathway, differing from MWAC by a high horizontal coefficient and mainly by the expansion factor occurring between the BC and the NAC. The specificity is even more outstanding due to differences with the null hypothesis. In comparison to the MWAC condensation which seems to be implied by the degree of the network due to low disparity with the randomized graphs, the NAC expansion does instead not originate from the degree distribution of the graph. Observing this, the network exhibits multiple possible information flow pathways: either expansion, condensation, or even a combination thereof through connections between the two Amacrine cell types. In the course of our study, we not only identified the cell and pathway that resolve the bottleneck hypothesis proposed by Nassi J. et al. (2), but we also unveiled an unexpected expansion pathway. We hypothesize that the expansion facilitates the extraction of specific visual features by generating parallel streams. This mechanism is analogous to what is observed in the field of computer vision with convolutional neural networks, where increasing the number of channels simplifies the features extraction.

While the topological analysis of the network has enabled us to uncover specific behaviors, we are aware that there is still room for improvement in modeling connectome networks. The dataset lacks the light-sensitive receptor cells, a key element in retinal processing, limiting the exploration of their connection with the BC rich-club. Additionally, the dataset contains little information on the types of synaptic connections, including the directions, the type of neurotransmitters, and the surfaces of contact. All these parameters will modify the dynamic of connections (19). However, the initial challenge in analysing this connectome network did not arise from the data but rather from a lack of mathematical foundations for accurate topological analysis. Most definitions of multilayer analysis focus on multiplex graphs without generalization to adjacency matrix equations. Expanding the application of the shortest pathway algorithm could be a useful next step to uncover additional topological properties in interconnected models. Finally, further investigation into the modularity model could yield interesting results, as it appears more correlated with the cell position than with the cell types (Appendix image 12). The next objective could be merging the modular and the multilayer models for a more precise network representation.

4. Conclusion

In general, the analysis of brain networks consistently uncovers an evolutional competitive selection process (1). The retinal network is forced to adapt to constraints imposed by the optic nerve bottleneck. This restriction enhances the emergence of diverse mechanisms like rich-club hubs, expansion, and condensation of information flow to correctly extract the information of a visual scene. As these topological properties are cell-type-specific, it was necessary to develop an interconnected multilayer model instead of a monolayer one. In a subsequent step, we extended mathematical definitions and developed a pipeline with three algorithms specifically designed for interconnected models. We highlighted two pathways: the medium/wide-field Amacrine cells mainly condensing the connections and the narrow Amacrine cells expanding the information flow.

After all of this, one may pose the question, "Why is it important to comprehend retinal processing in its entirety?". To this end, we must contemplate the potential impact that such analysis could exert on medicinal therapy, exemplified by

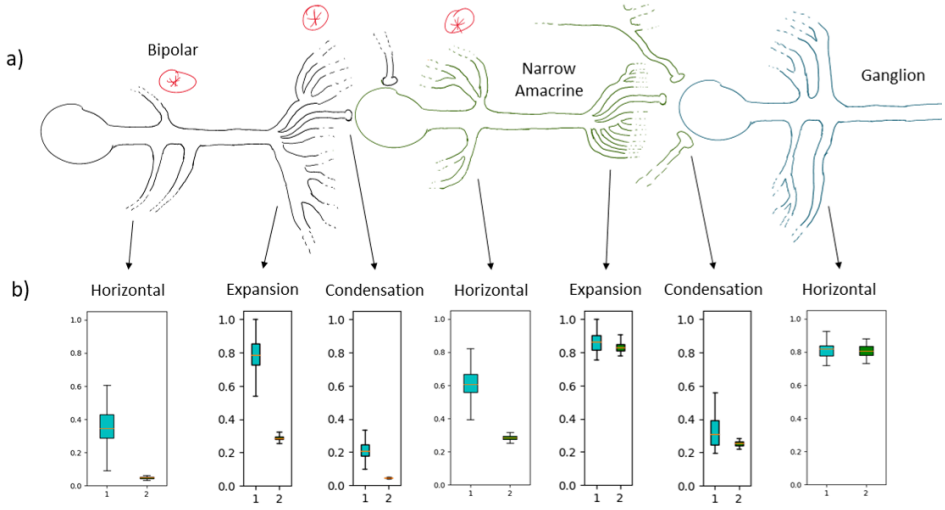

Fig. 7. The image illustrates the NAC pathway from the Bipolar to the narrow Amacrine, terminating in the Ganglion. a) Schematic of the possible specificity of the pathway. b) The variation of the local clustering coefficient during the pathway. The first column represents the original network, the second is the null hypothesis. NAC exhibits an early-stage expansion mechanism enhanced relative to the null hypothesis. Additionally, the horizontal local clustering coefficient is increased after this enlargement in the NAC layer. All specificities deviating from the null model are marked with a red star in (a), though they do not represent statistical evidence. The clustering coefficients in (b) are converted into the number of connections shown in (a), providing a conceptual idea of connections.

the Ophthalmic Translational Research Group of Professor Bence György at the Institute of Molecular and Clinical Opthalmology of Basel. Their use of viral therapy to induce light sensitivity in retinal cells for vision restoration is notable. Considering that targeting the rich-club cells might offer an avenue to enhance the effect of viral injection, this constitutes a sufficient reason to analyze retinal connectome networks and to expand the mathematical framework of interconnected multilayer graphs.

Materials and Methods

Dataset. The dataset originates from NeuroData website (20) and has been partially preprocessed by Eric Jona (21). From the properties of the neuronal connection, the network is extremely dense with multiple synapses between two cells (Appendix Image 8). For this reason, we decided to model the number of connections (i.e. synapses) as a weight. A visualization of the network is represented in the image 1 using the Pymnet python package (22).

Algorithm. To our knowledge, the three algorithms are the first ones capable of computing rich-club and local clustering coefficients while generating a randomized network only based on the super-adjacency matrix of a multilayer graph. For most of the algorithms, the dataset was transformed into an unweighted matrix to have a more efficient double-edge swap randomization (i.e. with a weighted matrix, the algorithm is constrained to exchange same-weight edges). All Algorithm pseudo-codes are visible in the Appendix (Mat-RC-Algo 1, Mat-ClustCoeff-Algo 2, and Mat-D-E-S-Algo 3). We decided to generate 20 types of random models per submatrix. The number of swaps is randomly selected between one to five times the number of edges already present in the graph. To ensure that the number of randomly generated graphs was not a limiting factor for the rich-club analysis, we performed the same analysis using 100 random graphs with increased numbers of swaps. After an extensive simulation, we obtained identical results.

ACKNOWLEDGMENTS. Special thanks to Samuel and Yasaman for addressing all my questions and providing me feedback.

1. B Papo, David, Complex network theory and the brain (2014).
2. JJ Nassi, EM Callaway, Parallel processing strategies of the primate visual system (2009).
3. M Helmstaedter, et al., Connectomic reconstruction of the inner plexiform layer in the mouse retina. *Nature* **500**, 168–174 (2013).
4. A Hernández, JM Amigó, Multilayer adaptive networks in neuronal processing. (2022).
5. B Bentley, et al., The Multilayer Connectome of Caenorhabditis elegans. *PLoS Comput. Biol.* **12** (2016).
6. S Boccaletti, et al., The structure and dynamics of multilayer networks (2014).
7. Z Hammoud, F Kramer, Multilayer networks: aspects, implementations, and application in biomedicine. *Big Data Anal.* **5** (2020).
8. M Kivelä, et al., Multilayer networks. *J. Complex Networks* **2**, 203–271 (2014).
9. C Presigny, *Characterization of multilayer networks : theory and applications to the brain.* (Sorbonne Université), (2023).
10. CJ Jeon, E Strettoi, RH Masland, *The Major Cell Populations of the Mouse Retina.* (1998).
11. LA Remington, Chapter 4 - Retina in *Clinical Anatomy of the Visual System (Second Edition).* (Butterworth-Heinemann, Saint Louis), pp. 55–86 (2005).
12. AG Purves D, *Neuroscience. 2nd edition.* (2001).
13. SA Bloomfield, B Völgyi, The diverse functional roles and regulation of neuronal gap junctions in the retina (2009).
14. S Fortunato, M Barthé, *Resolution limit in community detection.* Vol. 104, pp. 36–41 (2007).
15. L Lagnado, Retinal processing: Amacrine cells keep it short and sweet. *Curr. Biol.* **8**, 598–600 (1998).
16. SP Kuo, PP Chiang, AR Nippert, EA Newman, Spatial organization and dynamics of the extracellular space in the mouse retina. *J. Neurosci.* **40**, 7785–7794 (2020).
17. M Newman, *Networks.* (Oxford University Press) Vol. 1, (2018).
18. A Hagberg, P Swart, D S Chult, Exploring network structure, dynamics, and function using networkx. (2008).
19. M Kaiser, A tutorial in connectome analysis: Topological and spatial features of brain networks. *NeuroImage* **57**, 892–907 (2011).
20. J Vogelstein, *Neurodata Connectomes.* (visited 17.01.2024).
21. E Jona, *Github Circuitdata Mouse retina.* (2015).
22. M Kivelä, *Pymnet: Multilayer networks library for Python.* (2016).

Appendix

Algorithm 1 Mat-RC-Algo ▷ Return a vector of Rich-club coefficients for each degree

Require: Mat ▷ Matrix of size NxM
Ensure: $\Omega(k)$
  $degree_m \leftarrow \sum_{i=1}^{M} A_{ij}$
  $degree_n \leftarrow \sum_{j=1}^{N} A_{ij}$
  $k \leftarrow 0$
  $Max_k \leftarrow max(degree_n, degree_m)$
  while $k <= Max_k$ **do**
    $Booldeg_m \leftarrow degree_m > k$
    $Booldeg_n \leftarrow degree_n > k$
    $Ek \leftarrow Booldeg_n^T \times Mat \times Booldeg_m^T$
    $Nk_m \leftarrow \sum_{j=1}^{N} Booldeg_{mj}$
    $Nk_n \leftarrow \sum_{i=1}^{M} Booldeg_{in}$
    $Nk \leftarrow Nk_n + Nk_m$
    if $Mat = Mat^T$ **then** ▷ In case of Symmetrical Matrix (intralayer)
      $Nk \leftarrow \frac{Nk}{2}$
      $Ek \leftarrow \frac{Ek}{2}$
    $\Omega(k) \leftarrow \frac{2Ek}{Nk \times (Nk-1)}$
    $k \leftarrow k + 1$

Algorithm 2 Mat-ClustCoeff-Algo ▷ Return the local clustering coefficient for expansion or condensation

Require: $Intralayermatrix, Interlayermatrix$
Ensure: $Clustering\_Coefficient(v_i)$
  for v_i `in` $Interlayermatrix$ **do**
    $Nbr\_Triangle \leftarrow 0$
    $Matrice\_Triples \leftarrow v_i \otimes v_i$ ▷ Return the matrix revealing of triples
    $Tuples\_Triples \leftarrow return\_non\_zero\_idx(Matrice\_Triples)$ ▷ Return unique and sorted tuples of the index where the matrix is non-zero
    for tup_j `in` $Tuples\_Triples$ **do**
      if $Intralayermatrix[tup_j] = 1$ **then** ▷ The triple is closed→ Triangle
        $Nbr\_Triangle += 1$
      $Degree_{vi} \leftarrow \sum_{j=1}^{N} (v_i)_j$
    $Clustering\_Coefficient(v_i) \leftarrow \frac{2 * Nbr\_Triangle}{(Degree_{vi} * (Degree_{vi} - 1))}$

Algorithm 3 Mat-D-E-S-Algo ▷ Return a randomized version of the matrix (Code structure similar to Networkx function)

Require: $Matrix, Nbr\_swap$
Ensure: $Random\_Matrix$
  $swap = 0$
  $degree_1 \leftarrow \sum_{i=1}^{M} Matrix_{ij}$
  $degree_2 \leftarrow \sum_{j=1}^{N} Matrix_{ij}$
  $cdf_1 \leftarrow netowrkx.utils.cumulative\_distribution(degree_1)$ ▷ Return cumlative distribution function
  $cdf_2 \leftarrow netowrkx.utils.cumulative\_distribution(degree_2)$
  while $swap < Nbr\_swap$ **do**
    $u \leftarrow Return\_sample\_from(cdf1)$ ▷ Node from layer 1
    $x \leftarrow Return\_sample\_from(cdf2)$ ▷ Node from layer 2
    $Neighbor_u \leftarrow return\_index(Matrix[:, u])$ ▷ Return non-zero index corresponding to interlayer neighbors
    $Neighbor_x \leftarrow return\_index(Matrix[x, :])$
    $v \leftarrow random.choice(Neighbor_x)$
    $y \leftarrow random.choice(Neighbor_u)$
    if $Matrix[y, v] \neq 1$ and $Matrice[x, u] \neq 1$ **then** ▷ Check if none of these connections already existed
      $Matrix[x, v] = 0$
      $Matrix[y, u] = 0$
      $Matrix[x, u] = 1$
      $Matrix[y, v] = 1$

Nodes	GC	NAC	MWAC	BC
GC	35	215	206	461
NAC	215	180	351	606
MWAC	206	351	171	597
BC	461	606	597	426

Table 1. Nodes per layers. GC= ganglion cells, NAC= narrow amacrine cell, MWAC= medium/wide-field amacrine cell, BC= bipolar cell.

% Edges per layer	GC	NAC	MWAC	BC
GC	3.6	12.3	9.6	14.7
NAC	28.3	12	33.5	26.2
MWAC	31.2	47.2	18.7	49.4
BC	36.9	28.5	38.2	9.7
Total	12320	28432	40020	30922

Table 2. Percentage of Edges per layers. The last line is the total number of edges for the specific layer. GC= ganglion cells, NAC= narrow amacrine cell, MWAC= medium/wide-field amacrine cell, BC= bipolar cell

5. Python Code

The code and data are available on GitHub:
https://github.com/robinduvoisin/Multilayer_Retinal_Connectome_Analysis

6. Images

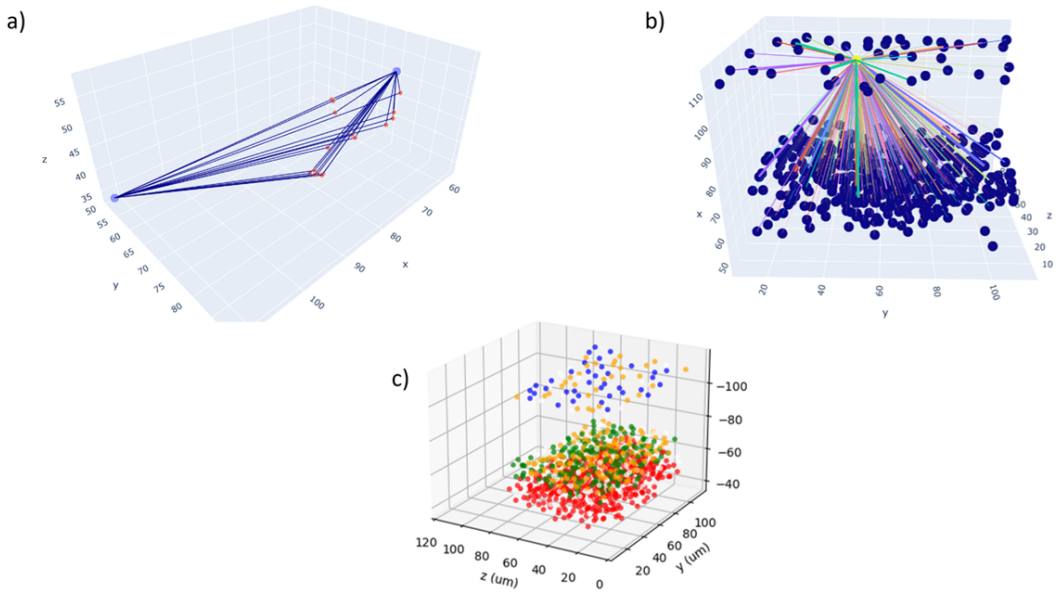

Fig. 8. 3D representation of the connectome. The x,y,z axes represent distances in µm. a) Illustration of the synaptic connections between two cells. The blue dot represents the cell, and the red dots depict synaptic connections. Saving the exact positions of all synapse connections for the entire network would be computationally heavy, thus we aggregated all synapses into a weight parameter. In this case, the weight would be 15. b) An example of all connections made by a randomly selected cell (yellow dot). The thickness of the line represents the weight of the connection. c) Visualization of cell position with color separation based on cell types: red dots for Bipolar cells, green dots for narrow Amacrine cells, orange for medium/wide-field Amacrine cells, and blue for Ganglion cells.

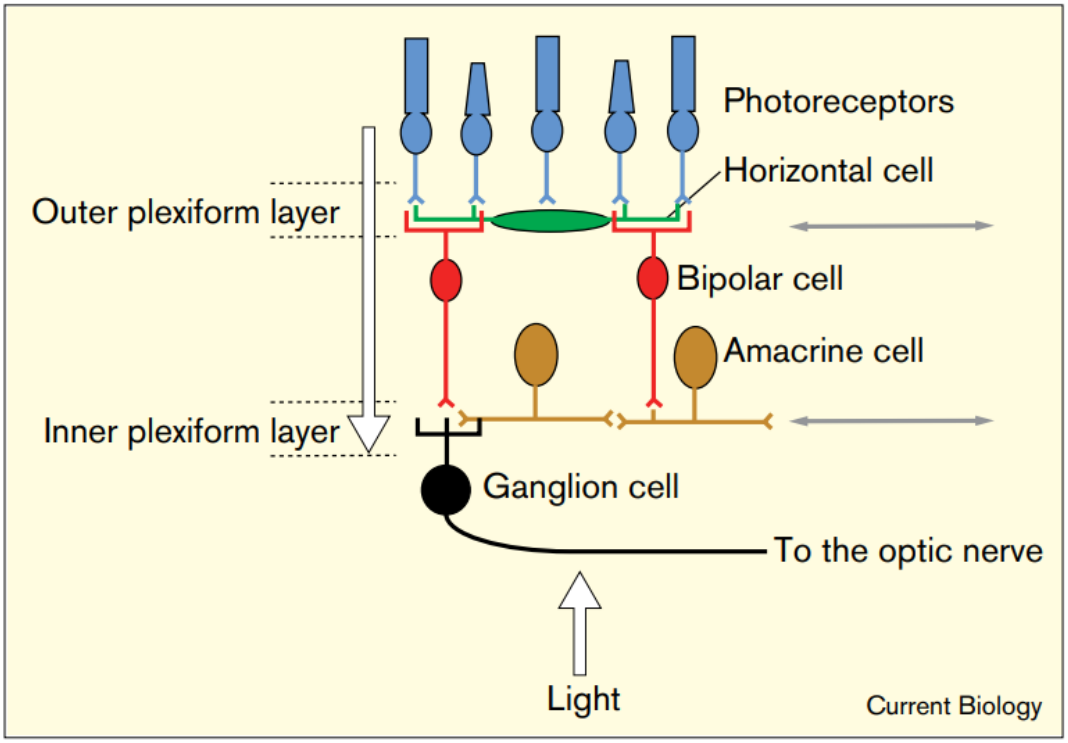

Fig. 9. The schematic depicts the retinal processing network, sourced from the article authored by L.Lagnado et al.(15). The connectome was limited to Bipolar, Amacrine, and Ganglion cells. We can observe the distinction between the vertical (BC and GC) and horizontal (AC) intervention of the cells.

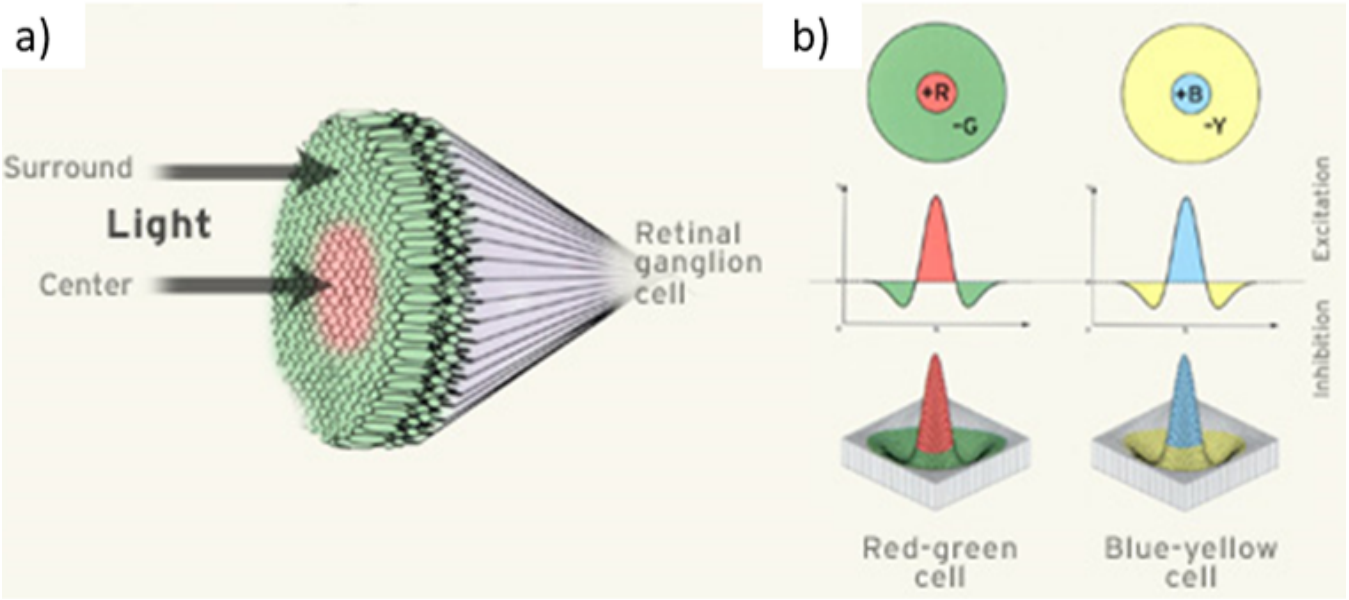

Fig. 10. The image is sourced from the website https://lavalle.pl/vr/node136.html by Steven M. LaValle (visited 18.02.2024). It illustrates the input that activates a typical ganglion cell. a) The light-sensitive receptor cell information undergoes condensation until it reaches a ganglion cell. The input from the receptor cells in the center of the field will be selective to a distinct feature compared to the receptor cells surrounding the field. b) The ganglion cell responds to a Difference of Gaussian input. This graph serves as an example of the input that would excite a type of Ganglion cell (i.e. a high red component in the middle that contrasts with a low green component in the surroundings or similar with yellow and blue)

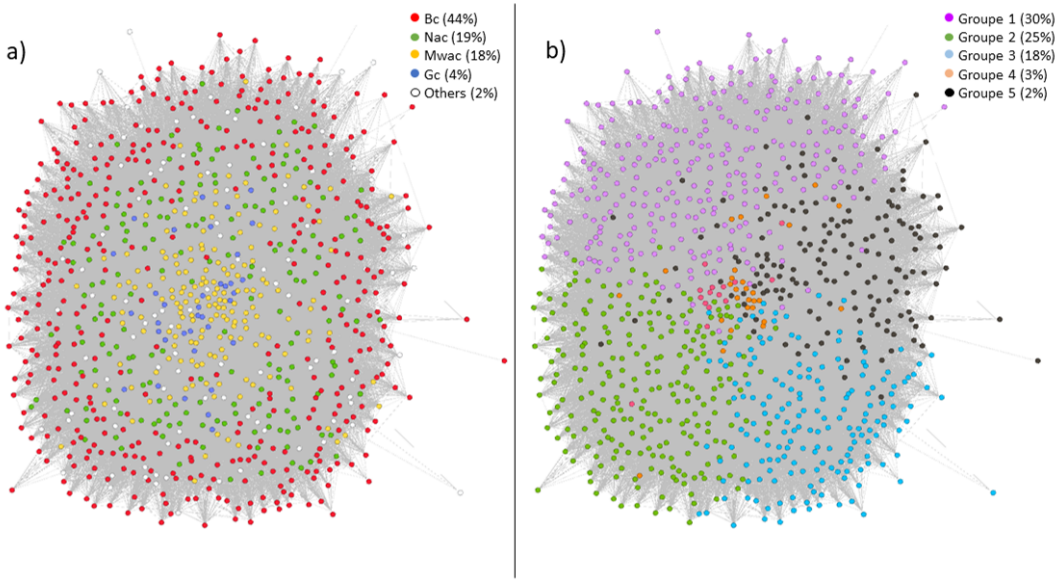

Fig. 11. Two representations of the monolayer graph from the dataset. a) Color classification based on cell type. b) Color classification using a community detection algorithm based on modularity with visualization by Gephi. The two segmentations do not tend to be correlated.

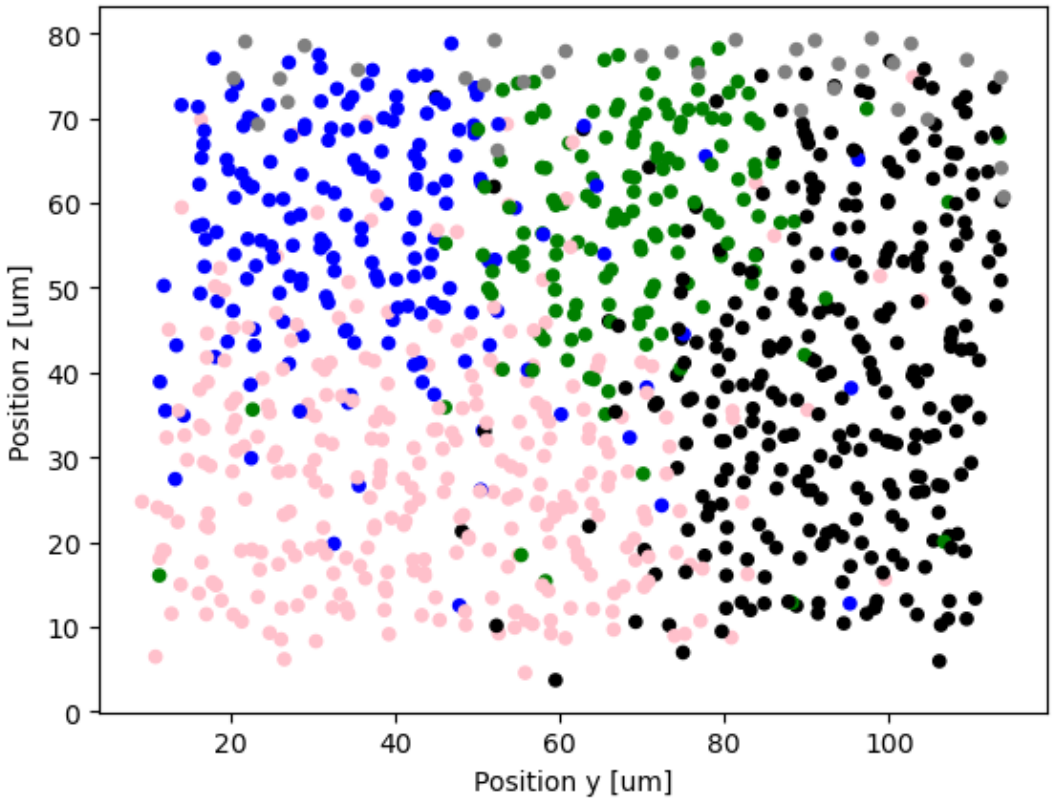

Fig. 12. The network is represented with nodes positioned correctly along the y and z axes with color segmentation based on community detection (image 11), where grey color replaces all smaller communities ($\leq$1% of the network). The modularity segmentation appears to be more correlated with the cell position than the cell type. This observation could indicate a columnar organization in the retinal network.

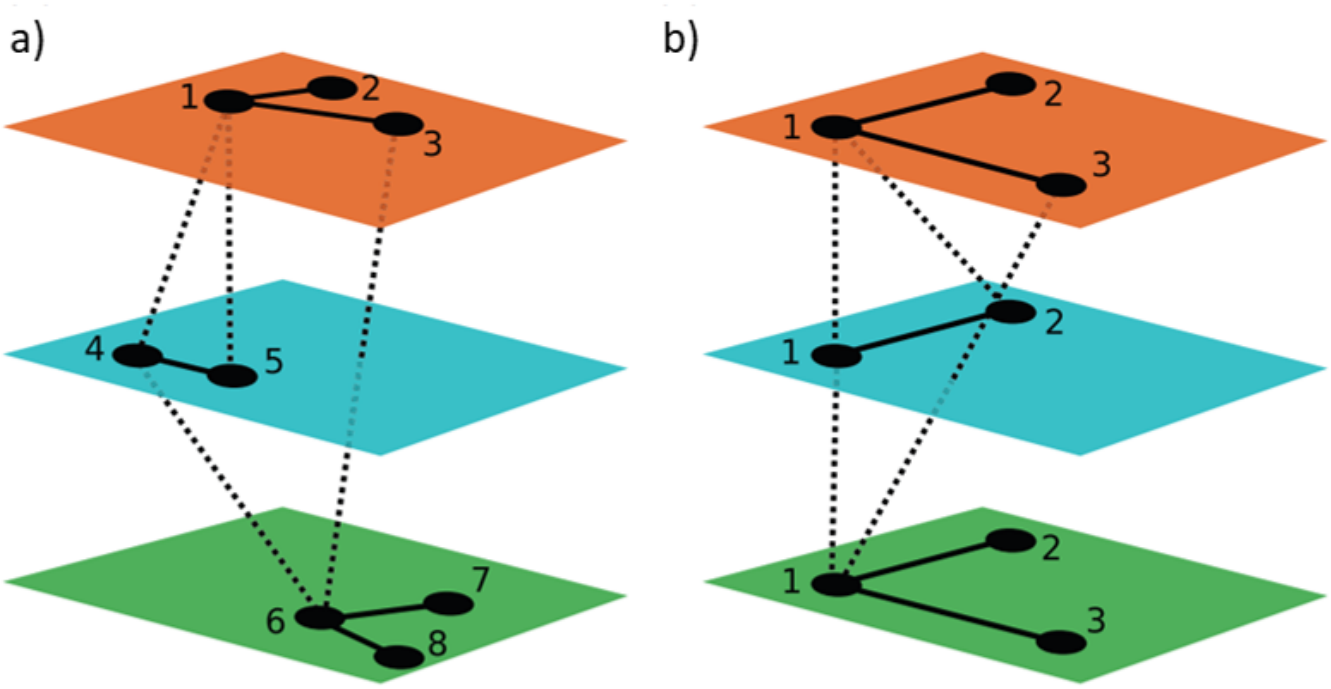

Fig. 13. The image originates from the article written by Kivelä et al.(8). It illustrates the difference between a) an interconnected network and b) a multiplex network.

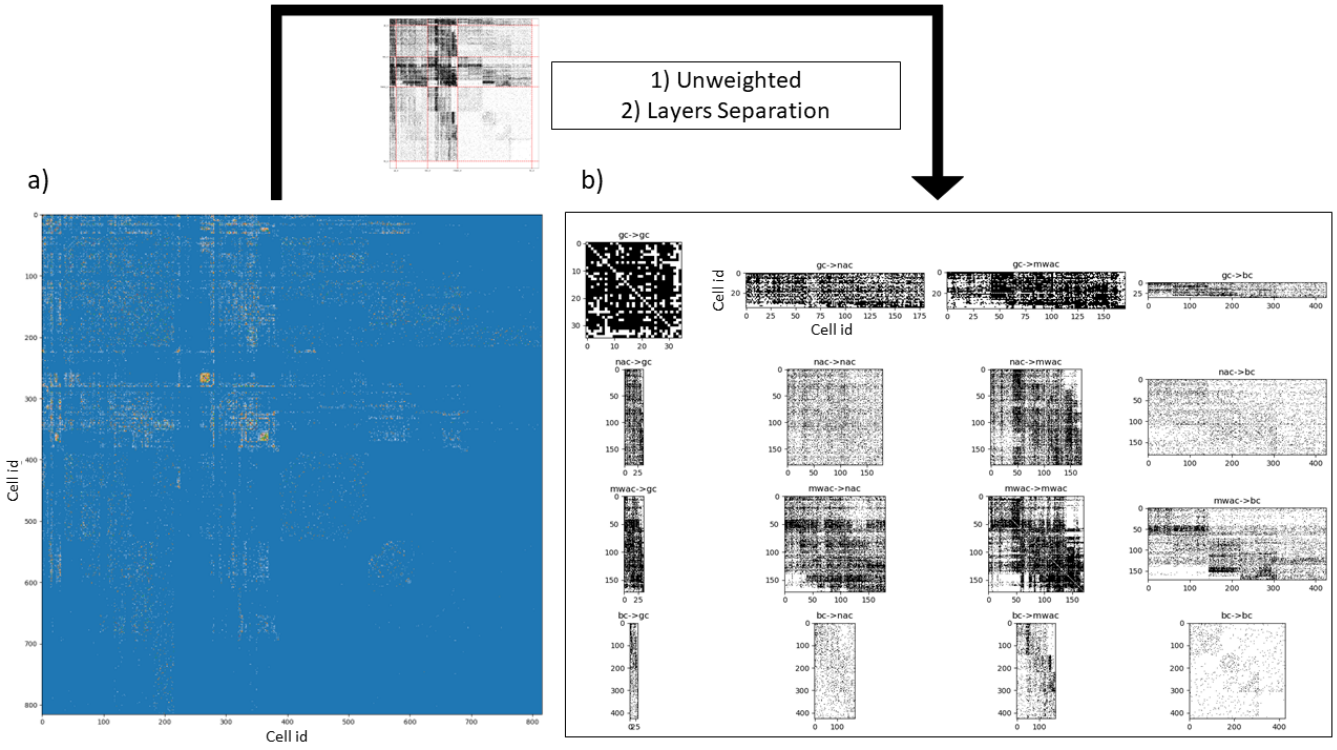

Fig. 14. The image is solely a schematic representation of the transformation from a monolayer to a multilayer model. a) The weighted supra-adjacency matrix is extracted from the connectome dataset. The weight is color-graded, where blue corresponds to no edges. The X and Y axes represent the cell ID numbers. b) The inter and intra matrices between each layer. These matrices are extracted from a) after an initial unweighted transformation, followed by separation based on cell types.

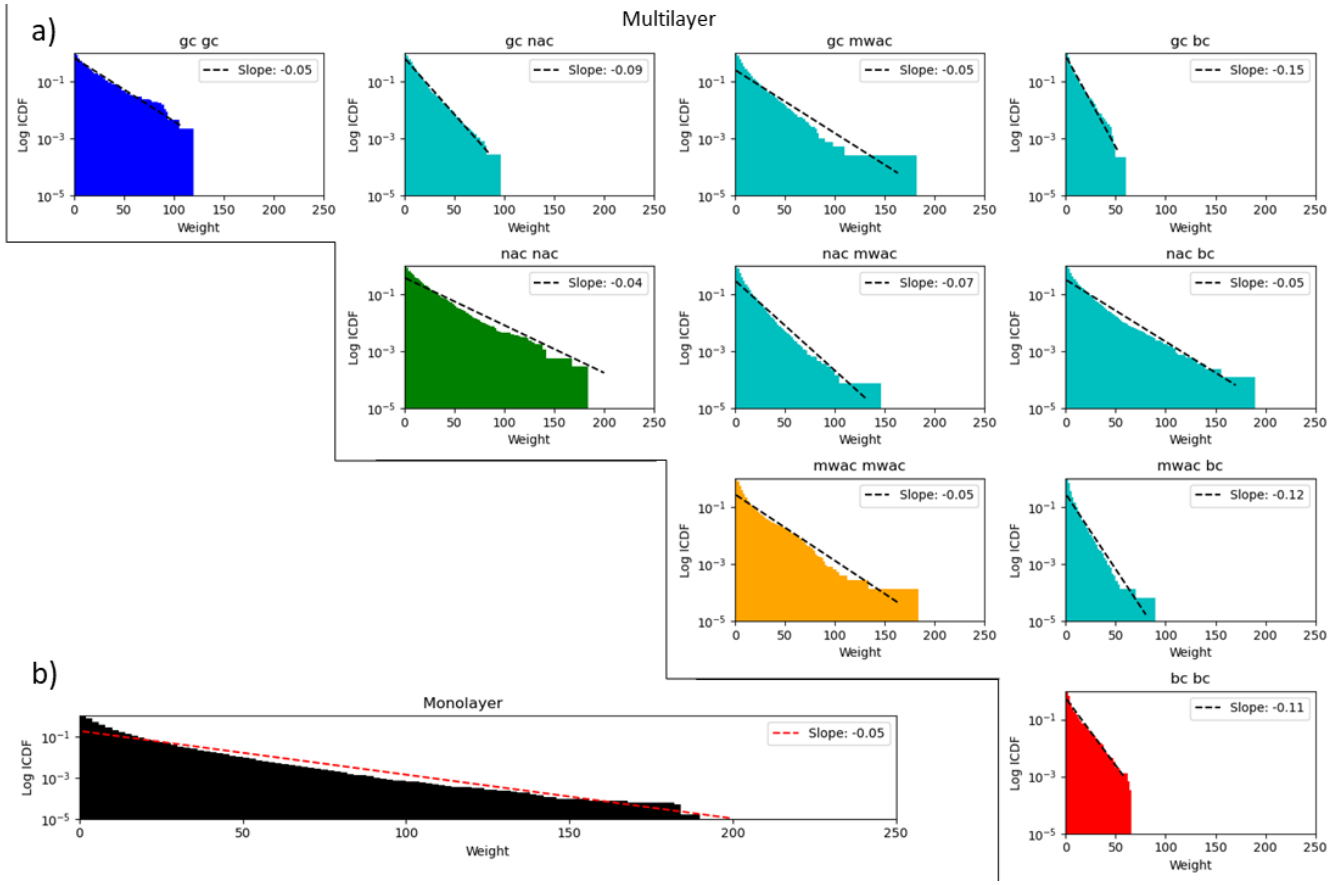

Fig. 15. a) Multilayer model: The weight logarithmic inversed cumulative distribution function of inter- and intralayers. The title indicates the two layers being analyzed. The curve represents a linear fit of the function, with the legend denoting the slope (i.e., since it's a log plot, the slope is, in reality, an exponential factor). b) Similar graph for the Monolayer model: The slope of the monolayer model does not encompass all the slopes observed in the multilayer model. This image reaffirms the inability to capture the network's behavior adequately through a monolayer model.

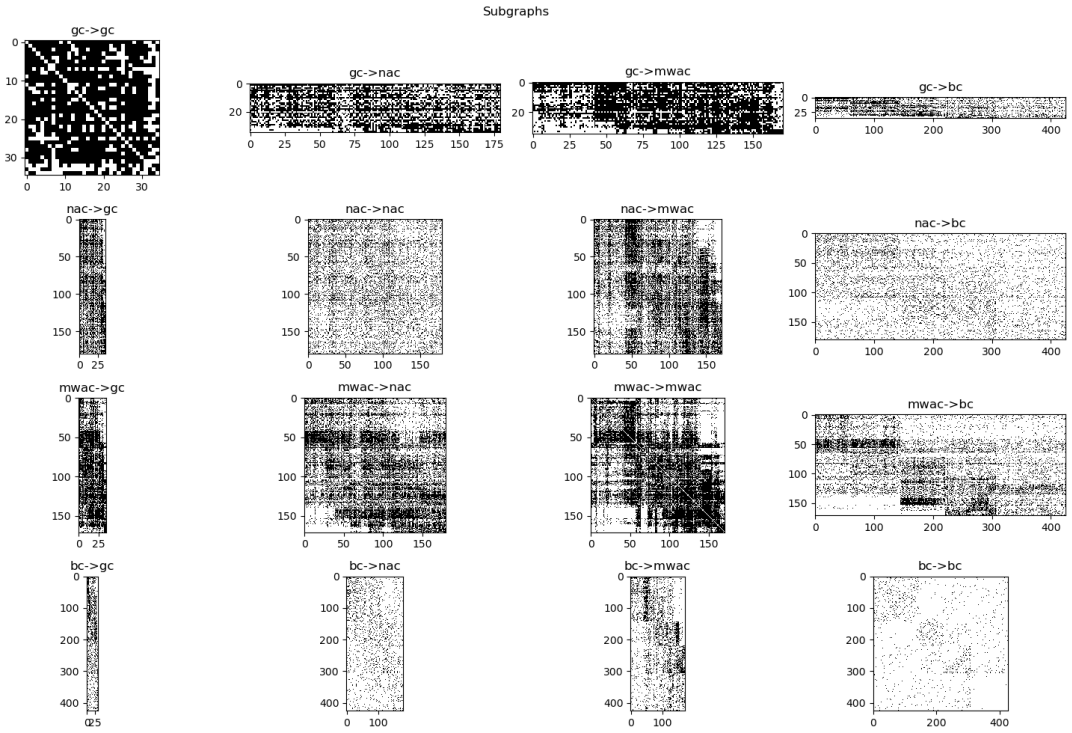

Fig. 16. The unweighted Supra-adjacency matrix of the connectome. The X and Y axes represent the cell identification number. GC= ganglion cell, BC= bipolar cell, NAC=narrow amacrine cell, MWAC= medium/wide-field amacrine cell.

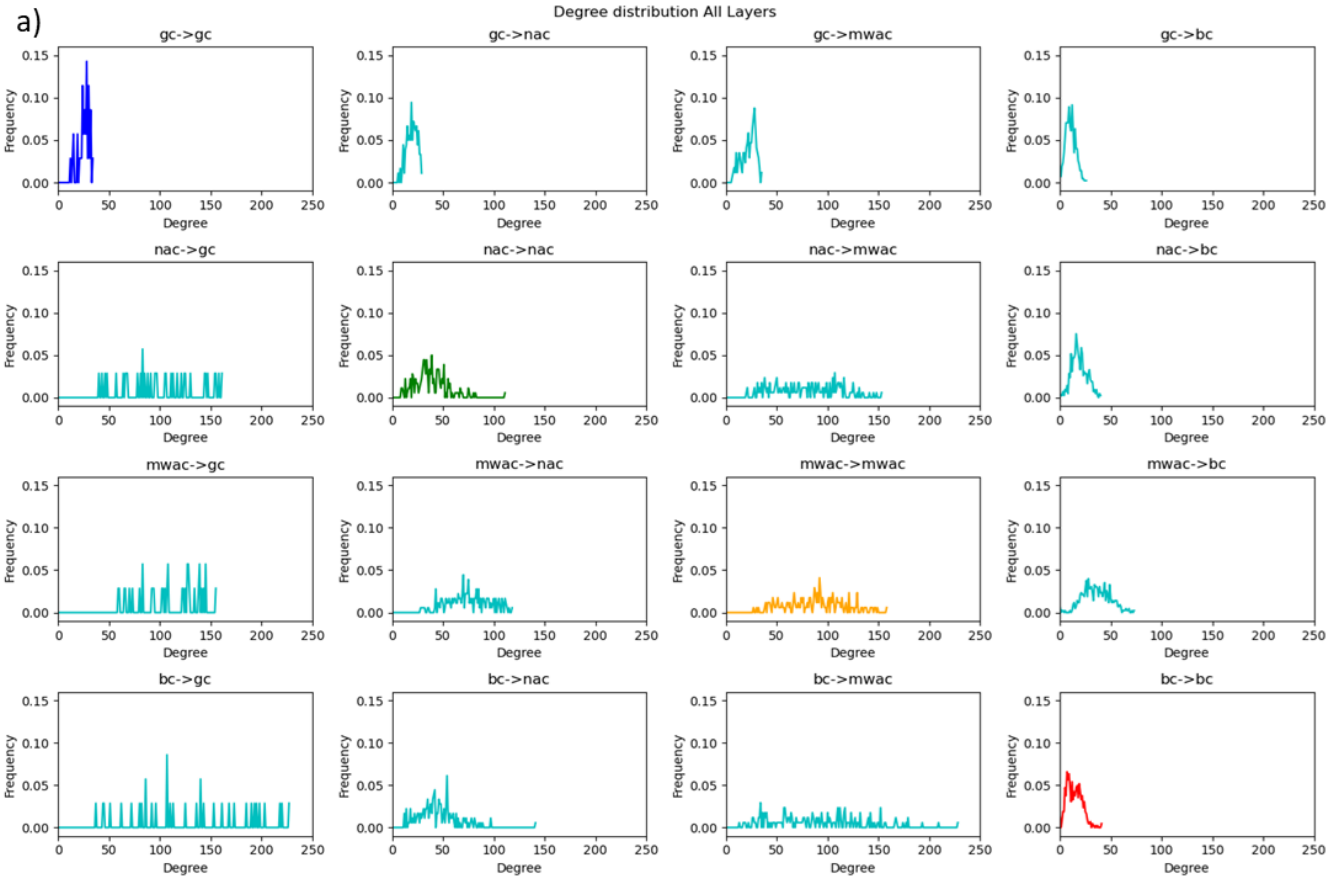

Fig. 17. Illustration of the degree distribution of inter- and intralayers. In the upper triangular part of the graph, we observe all connections from the Ganglion to the Amacrine, from the Ganglion to the Bipolar, and from the Amacrine to the Bipolar cells. These degree distributions exhibit a short variation near the peak, representing information flowing backward, commonly known as feedback. In the lower triangular part, we observe the feedforward dynamic, where information flows from the Bipolar to the Ganglion cells. These distributions are notably broader.

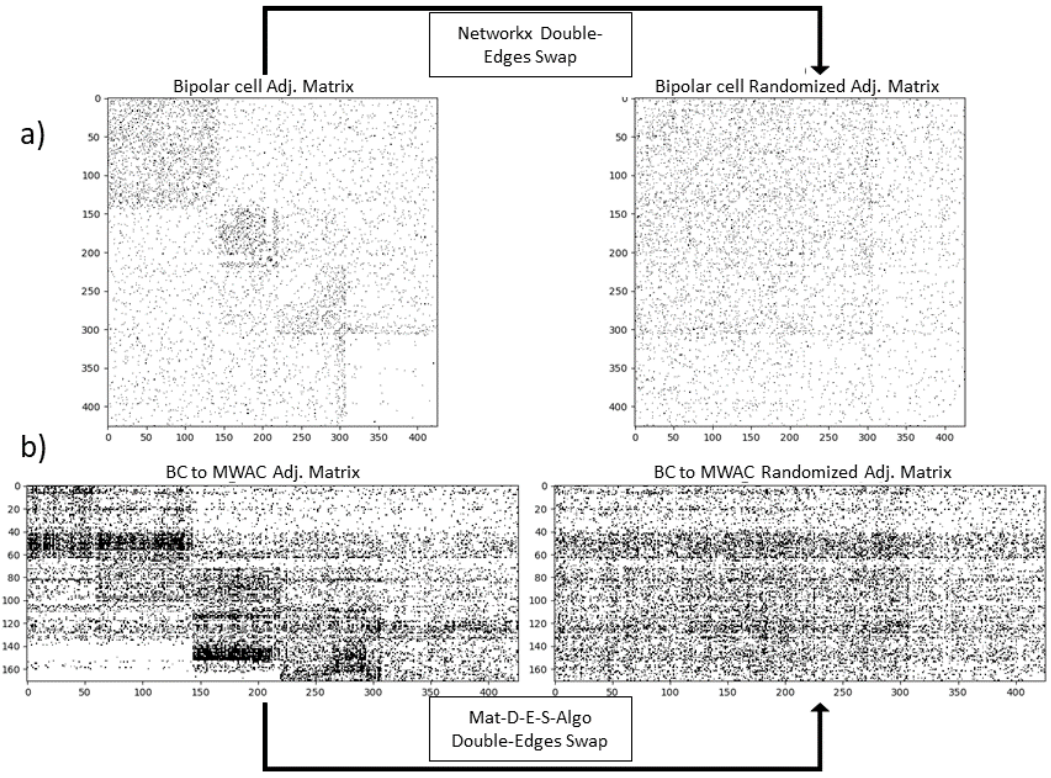

Fig. 18. a) The intralayer adjacency matrix of Bipolar cells before and after the double-edge swap algorithm from Networkx. The X and Y axes represent the cell identification number. b) The interlayer adjacency matrix between Bipolar and Amacrine cells before and after the double-edge swap performed by our algorithm Mat-D-E-S-Algo. It is evident that our algorithm is capable of randomizing a non-symmetrical matrix to later compare topological properties, such as rich-club, to a null model. The X and Y axes represent the cell identification number.

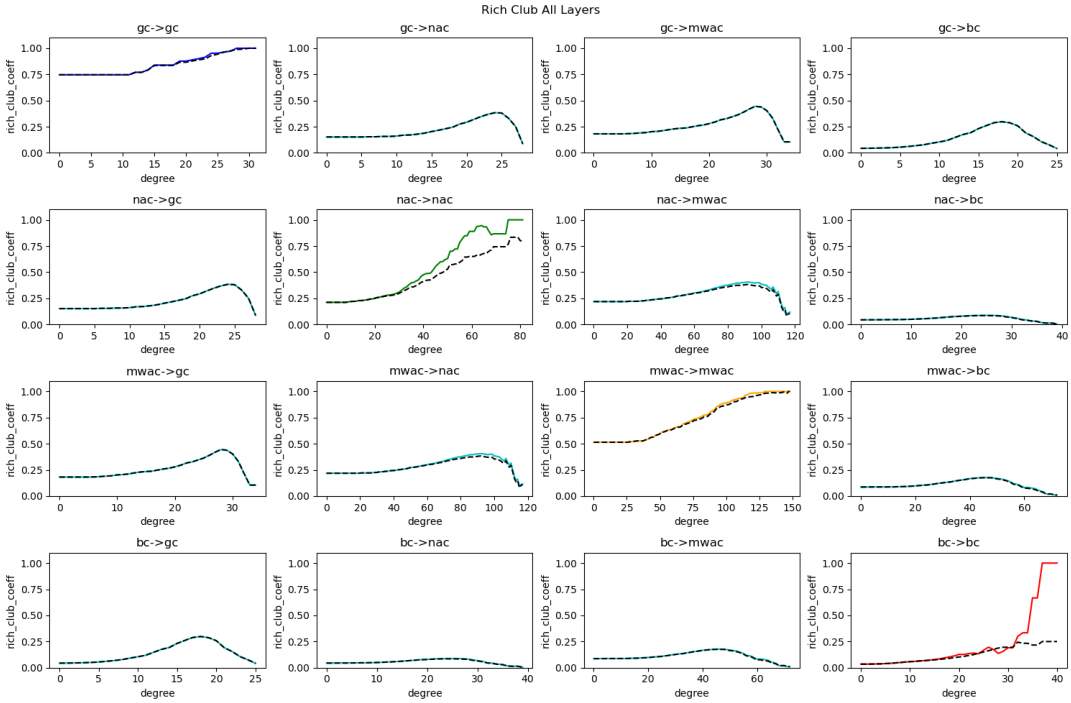

Fig. 19. All Rich-Club coefficients computed on the connectome network (red line) and on a randomized version of it (dashed black line). Any disparity between the two lines indicates that the rich-club coefficient is greater than 1, revealing a hub for that specific degree. GC=ganglion cell, NAC=narrow amacrine cell, MWAC=medium/wide-field cell, BC=bipolar cell.

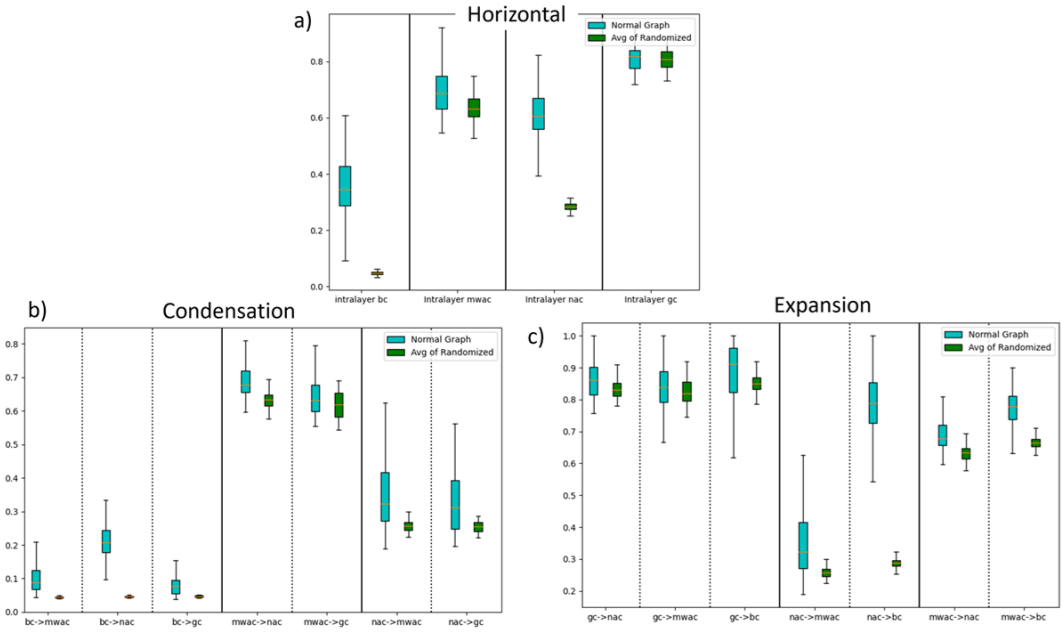

Fig. 20. All local clustering coefficients computed on the connectome network (blue) and on a randomized version of it (green). a) The Horizontal coefficient, specific to triangles on a single plane (intralayer). b) The condensation clustering coefficient represents triangles that initiate from an early layer in the retinal processing, involving two connected nodes that converge into one node in a late layer. c) The expansion originates from one node in an early stage of retinal computation, connected with two other nodes in a later stage. GC=ganglion cell, NAC=narrow amacrine cell, MWAC=medium/wide-field cell, BC=bipolar cell.